Lipid bilayers decorated with photosensitive ruthenium complexes

Bahreman, A.

Appendix I

General photochemistry methods

AI.1. Determination of the extinction coefficients

AI.1.1. Extinction coefficients of kinetically stable compounds in an aqueous solution

For a non-labile compound RuL (where L is a monodentate ligand, typically L=H_2O, or SRR') at room temperature the extinction coefficient was determined as follows:

A stock solution **α** of compound RuL was prepared (typical concentration:10^{-4} M) in water and by successive dilution of solution **α**, five or six solutions with different concentrations (typically between 10^{-4} and 10^{-5} M) were prepared. The UV-vis spectra of all samples were measured, typically between 350-700 nm. The extinction coefficient at each wavelength was then determined from the slope of the plot of absorbance *vs.* concentration according to Beer-Lambert Equation AI.1. In this equation l is the UV-vis absorbance pathlength, ε_{RuL} is the extinction coefficient of RuL, and *[RuL]* is the concentration of RuL.

$$A = \varepsilon_{RuL} \cdot l \cdot [RuL] \quad \textbf{(Equation AI.1)}$$

AI.1.2. Extinction coefficients of kinetically labile compounds involved in a fast thermodynamic equilibrium

When the ruthenium thioether complex RuSRR' is in a thermal equilibrium with the corresponding ruthenium aqua complex $RuOH_2$ (taking into account that none of H_2O or thioether ligands absorb light) determination of the extinction coefficient of RuSRR' requires a different method than of kinetically stable compounds. A stock solution **β** of thioether compound SRR' in water and a stock solution **δ** of RuSRR' in solution **β**, were prepared. Four solutions containing 3–x mL of solution **β** and x mL of solution **δ** were prepared, where x = 0.5, 1.0, 1.5 or 2 mL. UV-vis spectra were measured for all samples. In such conditions, the concentration in thioether SRR' compound is the same for all samples, so that the ratio $[RuSRR']/[RuOH_2]$ remains constant (Equation AI.2). However, due to dilution of the ruthenium complex (solution **δ**) with the SRR' solution (solution **β**), the total concentration in ruthenium $[Ru]_{tot}$ increases from x=0.5 to x=2. At constant $[RuSRR']/[RuOH_2]$ ratio, $[RuSRR']$ is proportional to $[Ru]_{tot}$ and can be calculated according to Equation AI.3.

$$K' = \frac{[RuSRR']}{[RuOH_2]} = K \cdot [RuSRR'] \quad \textbf{(Equation AI.2)}$$

$$r = \frac{[RuSRR']}{[Ru]_{tot}} = \frac{K'}{K' + 1} \qquad \textbf{(Equation AI.3)}$$

From the value of r in Equation AI.3 and the extinction coefficient of $RuOH_2$ which was determined using the method in section AI.1.1, the extinction coefficient of RuSRR' was calculated using Equation AI.4. In this equation ε_{eq} is the extinction coefficient obtained from the slope of the plot of the absorbance versus *[RuSRR']* at the equilibrium.

$$\varepsilon_{RuSRR'} = \frac{\varepsilon_{eq} - \left((1 - r) \cdot \varepsilon_{RuOH_2}\right)}{r} \qquad \textbf{(Equation AI.4)}$$

AI.2. Calculation of the concentration of the compounds from the UV-vis measurements

AI.2.1. One-wavelength method

There are two distinct methods for calculating the concentrations of two photochemically interconverting compounds in the solution by deconvolution of the UV-vis spectra. The first method needs one wavelength, at which the change in absorbance is large during the experiment. Another requirement for this method is that the reaction goes to completion. If we consider a substitution reaction RuSRR'+H_2O→ $RuOH_2$+SRR', after a given amount of time, all of RuSRR' is expected to be converted into $RuOH_2$ (assuming that H_2O and RSS' do not absorb light). The contribution of each compound to the absorbance of the solution (for each absorption measurement at t_j during the reaction) is a function of its concentration, the length of the cell, and the extinction coefficient of the compound, according to Beer-Lambert's law (see Equation AI.5).

$$A^{\lambda}_{t_j} = l \cdot \varepsilon^{\lambda}_{RuSRR'} \cdot [RuSRR'] + l \cdot \varepsilon^{\lambda}_{RuOH_2} \cdot [RuOH_2] \qquad \textbf{(Equation AI.5)}$$

If at t_∞, RuSRR' is fully converted into $RuOH_2$, thus the equation becomes:

$$A^{\lambda}_{t_\infty} = l \cdot \varepsilon^{\lambda}_{RuOH_2} \cdot [Ru]_{tot} \qquad \textbf{(Equation AI.6)}$$

$[Ru]_{tot}$ is the total Ru concentration. If we replace *$[RuOH_2]$* by *$[Ru]_{tot} - [RuSRR']$* in Equation AI.5, *[RuSRR']* can be obtained from Equation AI.7.

$$[RuSRR'] = \frac{A_{t_j}^{\lambda} - A_{t_\infty}^{\lambda}}{l \cdot \left(\varepsilon_{RuSRR'}^{\lambda} - \varepsilon_{RuOH_2}^{\lambda}\right)} \quad \textbf{(Equation AI.7)}$$

AI.2.2. Two-wavelength method

If the reaction does not go to completion, the absorbance at two different wavelengths λ_1 and λ_2 can be expressed as:

$$A_{t_j}^{\lambda_1} = l \cdot \varepsilon_{RuSRR'}^{\lambda_1} \cdot [RuSRR'] + l \cdot \varepsilon_{RuOH_2}^{\lambda_1} \cdot [RuOH_2] \quad \textbf{(Equation AI.8.a)}$$

$$A_{t_j}^{\lambda_2} = l \cdot \varepsilon_{RuSRR'}^{\lambda_2} \cdot [RuSRR'] + l \cdot \varepsilon_{RuOH_2}^{\lambda_2} \cdot [RuOH_2] \quad \textbf{(Equation AI.8b)}$$

Thus, *[RuSRR']* can be expressed as:

$$[RuSRR'] = \frac{A_{t_j}^{\lambda_1} - \left(l \cdot \varepsilon_{RuOH_2}^{\lambda_1} \cdot [RuOH_2]\right)}{l \cdot \varepsilon_{RuSRR'}^{\lambda_1}} \quad \textbf{(Equation AI.9)}$$

Equation AI.9 can be substituted in the Equation AI.8b, and *[$RuOH_2$]* can thus be expressed as a function of $A_{\lambda 1}$ and $A_{\lambda 2}$ to yield Equation AI.10 (with *l*= 1 cm).

$$[RuOH_2] = \frac{A_{t_j}^{\lambda_2} \cdot \varepsilon_{RuSRR'}^{\lambda_1} - A_{t_j}^{\lambda_1} \cdot \varepsilon_{RuSRR'}^{\lambda_2}}{\varepsilon_{RuSRR'}^{\lambda_1} \cdot \varepsilon_{RuOH_2}^{\lambda_2} - \varepsilon_{RuSRR'}^{\lambda_2} \cdot \varepsilon_{RuOH_2}^{\lambda_1}} \quad \textbf{(Equation AI.10)}$$

Calculation of concentrations and kinetic studies using the two-wavelength method depends on the accuracy of four extinction coefficients at two different wavelengths, whereas in the one-wavelength method only two extinction coefficients are needed. However, in the one-wavelength method the rate constant is highly sensitive to the accuracy of the absorbance at t_∞. In fact, if the reaction does not go to completion a wrong value is taken for $A_{t\infty}^{\lambda}$ and the accuracy of the calculated concentrations are slightly lower than the concentrations calculated with two-wavelength method.

AI.3. Photosubstitution quantum yield measurements

A.I.3.1. Irradiation close to an isosbestic point

For a photosubstitution reaction, where SRR' in RuSRR' is substituted by H_2O, assuming that the aqua complex $RuOH_2$ is not thermally reactive or photoreactive and that RuSRR' is

thermally stable in water and in the dark at room temperature, the photosubstitution quantum yield can be measured as follows:

The expression of the rate of the photosubstitution reaction is given by Equations AI.11 and AI.12, where $k_{\varphi i}$ is a first-order photosubstitution rate constant, $n_{RuSRR'}$ the number of moles of the RuSRR' complex at time *t*, φ_i the photosubstitution quantum yield, and $q_{RuSRR'}$ the number of moles of photons absorbed by the RuSRR' complex per unit time. $q_{RuSRR'}$ can be calculated using Equation AI.13, where Φ is the photon flux determined by standard ferrioxalate actinometry,[1] $1–10^{-Ae}$ is the probability of photon absorption, A_e is the absorbance of the solution at the irradiation wavelength, and $(A_{RuSRR'}/A_{Ru(tot)})$ the relative contribution of the RuSRR' complex to the total absorbance of the solution at the irradiation wavelength.

$$r_{photo} = \frac{dn_{RuSRR'}}{dt} = -k_{\varphi i} \cdot n_{RuSRR'} \qquad \textbf{(Equation AI.11)}$$

$$r_{photo} = -q_{RuSRR'} \cdot \varphi_i \qquad \textbf{(Equation AI.12)}$$

$$q_{RuSRR'} = \Phi \cdot (1 - 10^{-A_e}) \cdot \left(\frac{A_{RuSRR'}}{A_e}\right) \qquad \textbf{(Equation AI.13)}$$

If the irradiation wavelength λ_e is chosen close to the wavelength of the isosbestic point the probability of photon absorption remains constant during irradiation because $A_{RuSRR'}$ and A_e do not vary in time and at λ_e, $\varepsilon_e = \varepsilon_{RuSRR'} = \varepsilon_{Ru(tot)}$. Equations AI.12 and AI.13 rearrange to Equation AI.14, where $n_{Ru(tot)}$ is the total number of moles of ruthenium complexes in the UV-vis cuvette.

$$r_{photo} = \frac{dn_{RuSRR'}}{dt} = -\Phi \cdot (1 - 10^{-A_e}) \cdot \left(\frac{n_{RuSRR'}}{n_{Ru(tot)}}\right) \cdot \varphi_i \qquad \textbf{(Equation AI.14)}$$

By comparison between equation AI.11 and AI.14, quantum yield φ_i can be obtained from Equation AI.15.

$$\varphi_i = \frac{k_{\varphi i} \cdot n_{Ru_{(tot)}}}{\Phi \cdot (1 - 10^{-A_e})} \qquad \textbf{(Equation AI.15)}$$

Note 1: $k_{\varphi i}$ in Equation AI.15 can be obtained from the slope of a plot of $\ln([RuSRR']/[Ru]_{tot})$ *vs.* irradiation time (see Equation AI.11). For kinetically unstable RuSRR' complex in water, where RuSRR' and $RuOH_2$ are in a thermal equilibrium, another method is used to calculate $k_{\varphi i}$ (see Appendix III, section AIII.9).

AI.3.2. Irradiation at the wavelength that is not an isosbestic point

When the irradiation wavelength is not close to an isosbestic point, the absorbance at the irradiation wavelength is not constant throughout the irradiation, which must be taken into account. Thus the procedure below was applied to calculate the photosubstitution quantum yields.[2]

The average absorbance between two consecutive UV-vis measurements at t_j and t_{j+1}, at the irradiation wavelength λ_e, was calculated according to Equation AI.16.

$$(A_e)_{ave} = \frac{(A_e)_j + (A_e)_{j+1}}{2} \quad \textbf{(Equation AI.16)}$$

The number of moles of photons q_j absorbed by the ruthenium complex RuSRR' between two consecutive UV-vis measurements ($\Delta t = t_{j+1} - t_j$), was calculated according to Equation AI.17. In this Equation Φ is the photon flux at irradiation wavelength λ_e and $(1 - 10^{(A_e)ave})$ is the probability of photon absorption. If the sample was irradiated from the top of the cuvette ($l' = 3\ cm$), while the absorbance was measured perpendicular to the light irradiation direction (absorbance pathlength l=1 cm), A_e must be multiplied by 3 (see Figure AI.1).

$$q_j = \left(\frac{A_{RuSRR'}}{(A_e)_{ave}}\right)_j \cdot \left(1 - 10^{-(A_e)ave}\right) \cdot \Phi \cdot \Delta t \quad \textbf{(Equation AI.17)}$$

The total number of moles of absorbed photons since t_0 ($t_0 \rightarrow t_j$), Q_j, can then be calculated at each irradiation time according to Equation AI.18.

$$Q(t) = \sum_j q_j \quad \textbf{(Equation AI.18)}$$

Finally, the quantum yield φ_i can be obtained from the slope of a plot of the number of moles of RuSRR'($n_{RuSRR'}$) *vs.* Q_j.

Note 2: probability of absorbance depends on the irradiation pathlength (l'). If the sample is irradiated from the top of the UV-vis cuvette l'=3 cm (see Figure AI.1), A_e, which is

measured by a spectrometer over a pathlength of l cm, must be multiplied by 3. Thus in Equation AI.15 and AI.17 probability of absorbance is: $(1-10^{-(Ae\times 3)})$.

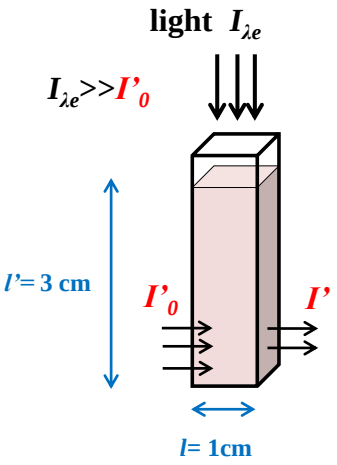

Figure AI.1. Irradiation of a solution in a UV-vis cuvette is done *in situ*, perpendicular to the optical axis of the spectrophotometer. Irradiation pathlength=l', UV-vis absorption pathlength=l, $I_{\lambda e}$: light power at irradiation wavelength λ_e. I': UV-vis light beam intensity measured by the spectrophotometer.

AI.4. References

[1] J. G. P. Calvert, J. N., *Chemical actinometer for the determination of ultraviolet light intensities. In Photochemistry.* Wiley and Sons, New York, **1967**, 780**.**

[2] M. Rougee, T. Ebbesen, F. Ghetti, R. V. Bensasson, *J. Phys. Chem.* **1982**, *86*, 4404.

Appendix II

Supporting Information of Chapter 2:

Ruthenium polypyridyl complexes hopping at anionic lipid bilayers *via* a supramolecular bond sensitive to visible light

AII.1. Synthesis

Dcbpy: 6,6-dibromo-2,2'-bipyridine (800 mg, 2.56 mmol) and PCl_5 (2.64 g, 12.68 mmol) were dissolved in $POCl_3$ (26 mL). To this solution was added KI (0.26 g, 1.57 mmol). The solution was heated to reflux for 48 hours after which $POCl_3$ was distilled under vacuum. Water was slowly added to the residue after which the suspension was basified using concentrated aqueous ammonia. The suspension was extracted twice with DCM, the organic phase dried with $MgSO_4$, filtered and the filtrate evaporated under reduced pressure. The white solid was recrystallized twice from toluene to yield 6,6-dichloro-2,2'-bipyridine (393 mg, 68%). Characterization was identical to the reference.[1]

[Ru(terpy)(dcbpy)Cl]Cl ([3]Cl): [Ru(tpy)Cl_3] (67.1 mg, 0.15 mmol) and dcbpy (58.7 mg, 0.26 mmol) were dissolved in ethylene glycol (1 mL). The mixture was heated to 180 °C for 4 hours, after which EtOH (2 mL) was added. The mixture was filtered to remove insoluble material and the filtrate was put under reduced pressure to remove EtOH. The purple solution was purified over neutral alumina (eluent: 95:5 DCM/MeOH); excess ethylene glygol was removed by coevaporation with toluene. The product was finally reprecipitated from MeOH/Et_2O to yield [**3**]Cl as a violet powder (47.5 mg, 50%). *^{1}H NMR (300 MHz, MeOD, see Scheme 2.1 for proton notation)* δ 8.75 (d, *J* = 8.1 Hz, 1H, B3), 8.54 (d, *J* = 8.1 Hz, 2H, T3'5'), 8.51 – 8.41 (m, 3H, T33"+A3), 8.32 (t, *J* = 8.0 Hz, 1H, B4), 8.18 – 8.03 (m, 4H, T66"+T4'+B5), 8.00 (td, *J* = 7.9, 1.4 Hz, 2H, T44"), 7.72 (t, *J* = 8.0 Hz, 1H, A4), 7.45 (dd, *J* = 9.6, 3.6 Hz, 2H, T55"), 7.17 (d, *J* = 7.9 Hz, 1H, A5). *^{13}C NMR (75 MHz, $CDCl_3$)* δ 166.17+160.93+160.27+ 160.21+159.75+159.22 (B6+B2+A2+A6+T22"+T2'6'), 153.86 (T66"), 139.76 (B4), 138.39 (A4), 137.82 (T44"), 135.54 (T4'), 128.77 (B5), 127.44 (A5), 127.15 (T55"), 123.47 (T33"), 122.81 (A3), 122.55 (B3), 122.28 (T3'5'). *ES MS m/z (calc):* 595.9 (534.86 $[M - Cl^-]^+$), 295.7 (295.7 $[M - 2\ Cl + MeOH]^{2+}$). *Anal. Calcd for $C_{25}H_{17}Cl_4N_5Ru{\cdot}4H_2O$*: C, 42.75; H, 3.59; N, 9.97. Found: C, 42.90; H, 3.01; N, 10.05.

[Ru(terpy)(dcbpy)(H_2O)](PF_6)$_2$ ([1](PF_6)$_2$): [**3**]Cl (50 mg, 85 μmol) and $AgPF_6$ (65 mg, 0.26 mmol) were dissolved in 4:1 acetone/H_2O (5 mL). The solution was shortly heated to boiling point and allowed to cool down. The solution was filtered over *celite*, concentrated under reduced pressure to 1 mL, after which it was put in the fridge overnight. The suspension was filtered to yield [**1**](PF_6)$_2$ as a brown powder (42.7 mg, 58%). ^{1}H NMR (300 MHz, D_2O, 298 K) δ 8.66 (d, *J* = 8.2 Hz, 1H, B3), 8.51 (d, *J* = 8.1 Hz, 2H, T3'5'), 8.43 (d, *J* = 8.0 Hz, 2H, T33"), 8.38 – 8.27 (m, 2H, B4+A3), 8.21 (t, *J* = 8.1 Hz, 1H, T4'), 8.13 (d, *J* = 5.5 Hz, 2H, T66"), 8.10 – 7.93 (m, 3H, B5+T44"), 7.66 (t, *J* = 8.0 Hz, 1H, A4), 7.45 (ddd, *J* = 7.0, 5.7, 1.1 Hz, 2H, T55"), 7.12 (d, *J* = 8.0 Hz, 1H, A5). *UV-vis:* λ_{max} (ε in $L{\cdot}mol^{-1}{\cdot}cm^{-1}$) in H_2O: 488 nm (7550). *ES MS m/z (calc):* 590.0 (590.45 $[M - 2\ PF_6 - H_2O + MeO]^+$). ^{13}C NMR was impossible due to the poor solubility of [**1**](PF_6)$_2$ in D_2O.

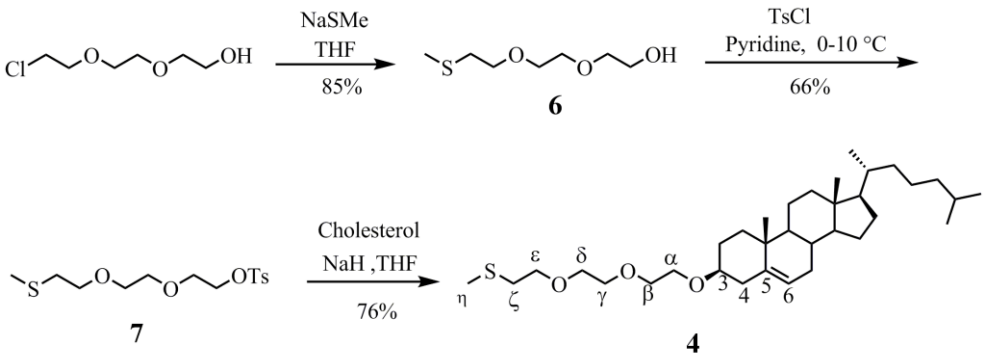

Scheme AII.1. Synthesis of ligand **4** and atom numbering scheme for NMR athribution.

6: A suspension of NaSMe (6.40 g, 91.3 mmol) in dry tetrahydrofuran (200 mL) was prepared under argon. While stirring 2-[2-(2-chloroethoxy)ethoxy]ethanol (9.62 g, 57.1 mmol) was added to the flask. The reaction mixture was refluxed under argon overnight and the solvent was evaporated under reduced pressure. The crude light yellow oil was dissolved in dichloromethane (130 mL) and washed with water (80 mL) and brine (2 × 80 mL). The organic layer was dried with $MgSO_4$ and concentrated under reduced pressur to give **6** as a colorless oil (8.80 g, 85%). ^{1}H NMR (300 MHz, δ in $CDCl_3$): 3.76-3.62 (m, 10H, α + β + γ + δ + ε), 2.71 (t, 2H, ζ), 2.46 (s, 1H, OH), 2.15 (s, 3H, η). ^{13}C NMR (75 MHz, δ in $CDCl_3$): 72.39 + 70.39 + 70.29 + 70.22 (α + β + γ + δ), 61.67 (ε), 33.35 (ζ), 15.94 (η). ES MS m/z (calc): 180.1 (180.3, $[M+Li]^+$).

7: To a solution of **6** (2.20 g, 12.2 mmol) in pyridine (10 ml) at 0 °C was added 4-toluenesulfonyl chloride (2.60 g, 13.6 mmol). The reaction mixture was left to stir at 0 °C for 3 h and at 10 °C for an additional 3.5 h. Toluene (30 ml) and HCl 10% (30 ml) were added. After drying the organic layer with MgSO4, the solvent was evaporated to yield **7** as light yellow oil (2.7 g, 66%). ^{1}H NMR (300 MHz, δ in $CDCl_3$): 7.80 (d, J = 8.2 Hz, 1H, CH-tosylate), 7.34 (d, J = 8.0 Hz, 1H, CH-tosylate), 4.16 (t, 2H, α), 3.76 – 3.50 (m, 8H, α + β + γ + δ), 2.67 (t, J = 6.8 Hz, 2H, ζ), 2.44 (s, 1H, η), 2.13 (s, 1H, CH_3-tosylate). ^{13}C NMR (75 MHz, δ in $CDCl_3$): 144.93, 133.17, 129.95, 128.12, 70.91 + 70.74 + 70.38 + 69.35 + 68.89 (α + β + γ + δ + ε), 33.59 (ζ), 21.68, 16.07 (η). ES MS m/z (calc): 357.1 (357.0, $[M+Na]^+$), 373.2 (373.2, $[M+K]^+$).

4: A suspension of sodium hydride (0.22 g, 9.2 mmol) in dry tetrahydrofuran (40 mL) was prepared under argon. While stirring, cholesterol (1.20 g, 3.10 mmol) was added to the flask. After 30 min, compound **7** (1.32 g, 3.95 mmol) in dry tetrahydrofuran (5 mL) was added to the mixture. It was then heated to reflux under argon for 48 h. The flask was cooled to room temperature and 60 mL of a (1:1) mixture of water and HCl 1 M was added.

The product was extracted three times with diethylether: petroleum ether 1:15 (v/v) (40 mL). The combined organic layers were washed once with HCl 1 M (30 mL), mixtures dried with $MgSO_4$ and finally evaporated off to give compound **4** as a sticky white solid (1.31 g, 76%). ^{1}H NMR (300 MHz, , δ in $CDCl_3$): 5.34 (d, J = 5.1 Hz, 1H, 6), 3.74 – 3.57 (m, 10H, α + β + γ + δ + ε), 3.17 (m, 1H, 3), 2.69 (t, J = 6.9 Hz, 2H, ζ), 2.42 – 2.19 (m, 2H), 2.14 (s, 3H, η), 2.05 – 0.81 (m, 42H), 0.67 (s, 3H). ^{13}C NMR (75 MHz, δ in $CDCl_3$): 141.17 (C5), 121.70 (C6), 79.67 (C3), 71.58 + 71.13 + 70.81 + 70.51 (α + β + γ + δ), 67.48 (ε), 56.96, 56.34, 50.37, 42.49, 39.97, 39.68, 39.25, 37.42, 37.04, 36.36, 35.94, 33.61, 32.12 (ζ), 32.07, 28.54, 28.39, 28.17, 24.45, 23.99, 22.96, 22.71, 21.24, 19.54, 18.88, 16.20 (η), 12.02. High resolution ES MS m/z exp (calc): 549.43413 (549.43413, $[M + H]^+$), 566.46068 (566.45998, $[M + NH_4]^+$), 571.41608 (571.41482, $[M + Na]^+$). *Anal. Calcd for* $C_{34}H_{60}O_3S$: calculated: C, 74.39; H, 11.02; N, 0.00; S, 5.84. Found: C, 74.39; H, 11.16; N, 0.0; S, 5.85.

AII.2. X-ray crystallography for [2](PF$_6$)$_2$

All reflection intensities were measured at 110(2) K using a KM4/Xcalibur (detector: Sapphire3) with enhance graphite-monochromated Mo *K*α radiation (λ = 0.71073 Å) under the program CrysAlisPro (Version 1.171.34.36, Oxford Diffraction Ltd., 2010). The program CrysAlisPro was used to refine the cell dimensions. Data reduction was done using the program CrysAlisPro (Version 1.171.34.36, Oxford Diffraction Ltd., 2010). The structure was solved with the program SHELXS-97[2] and was refined on F^2 with SHELXL-97.[2] Analytical numeric absorption corrections based on a multifaceted crystal model were applied using CrysAlisPro. The temperature of the data collection was controlled using the system Cryojet (manufactured by Oxford Instruments). The H atoms were placed at calculated positions using the instructions AFIX 23, AFIX 43, AFIX 137 with isotropic displacement parameters having values 1.2 or 1.5 times *U*eq of the attached C atoms. The H atom located on O1 was found from difference Fourier maps, and its position was restrained so that *d*(O–H) is 0.84(2) Å. The structure of [**2**](PF$_6$)$_2$ is mostly ordered. One of the two independent PF_6^- counterions is found to be disordered over two orientations, and the occupancy factor of the major component refines to 0.60(3).

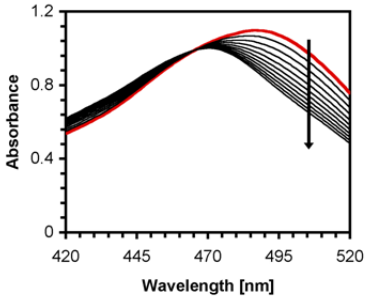

Figure AII.1. Time evolution of the UV-vis spectrum of a solution containing $[Ru(terpy)(dcbpy)(H_2O)]^{2+}$ ($[\mathbf{1}]^{2+}$) and Hmte in pseudo-first order conditions.

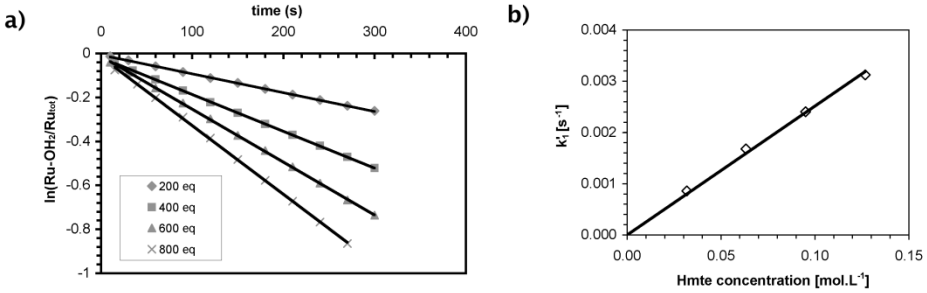

Figure AII.2. a) Plot of $ln([RuOH_2]/[Ru]_{tot})$ *vs*. time for 200, 400, 600 and 800 eq. of Hmte (pseudo-first order conditions). b) Plot of k'_1 *vs*. [Hmte] in pseudo-first order conditions. Conditions: T = 297 K; $[Ru]_{tot} = 1.4\times10^{-4}$ M.

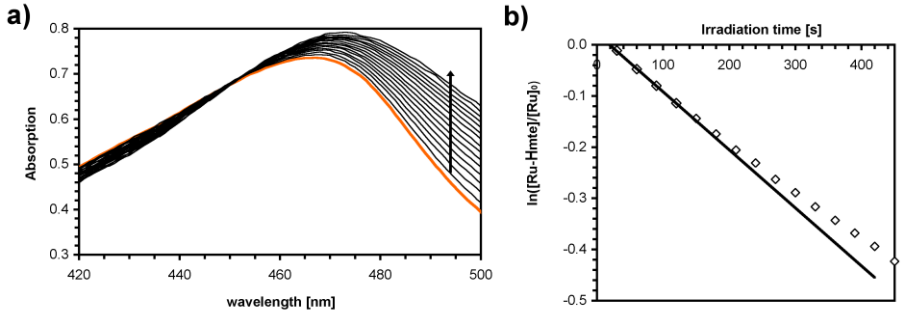

Figure AII.3. a) UV-vis spectra of a solution of $[\mathbf{2}](PF_6)_2$ in water irradiated at 465 nm. b) Plot of $ln([RuHmte]/[Ru]_{tot})$ as a function of irradiation time. Conditions: λ_e = 465 nm, photon flux :3.9×10^{-9} Einstein·s^{-1}, sample temperature 297 K, concentration $[Ru]_{tot} = 1.5\times10^{-4}$ M, spectra measured at 30 seconds interval.

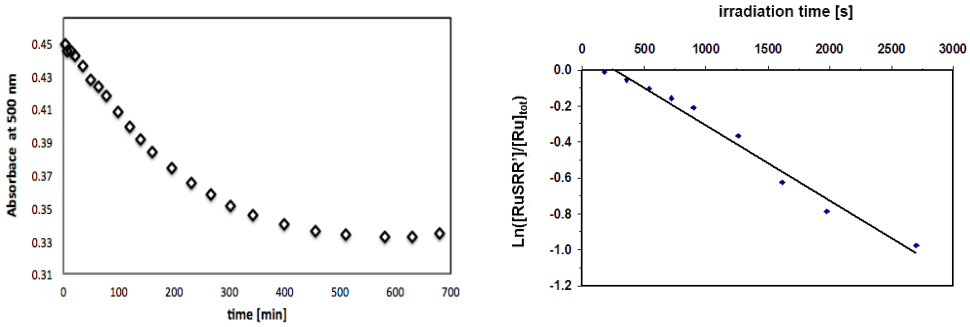

Figure AII.4. Left: Time evolution of the absorbance at 500 nm, for a sample containing DMPG vesicles with 25 mol % ligand **4**, and 5 mol % complex $[\mathbf{1}]^{2+}$ after equilibration at room temperature in the dark, spectra measured every 3 minutes. Right: Plot of $\ln(\textit{[RuSRR']/[Ru]}_{tot})$ *vs.* irradiation time for the measurement of the photosubstitution quantum yield at the membrane interface; *[RuSRR']* represents the concentration in $[\mathbf{5}]^{2+}$ in mol·L^{-1}. Conditions: *[lipid]* = 1.3 mM, 25 mol% of ligand **4**, vesicle average diameter 140 nm, 5 mol% of complex $[\mathbf{1}]^{2+}$ (6.7×10^{-5} M), irradiation wavelength 465 nm, photon flux :3.9×10^{-9} Einstein·s^{-1}.

AII.3. References

[1] E. C. Constable, K. R. Seddon, *Tetrahedron* **1983**, *39*, 291.
[2] G. M. Sheldrick, *Acta Crystallogr.* **2008**, *A64*, 112.

Appendix III

Supporting Information of Chapter 3:

Spontaneous formation in the dark, and visible light-induced cleavage, of a Ru-S bond in water: a thermodynamic and kinetic study

AIII.1. Synthesis

[Ru(terpy)(biq)(Cl)]Cl ([10]Cl).[1] [Ru(tpy)Cl_3] (200 mg, 0.453 mmol) and 2,2'-biquinoline (116 mg, 0.452 mmol) were mixed in 3:1 EtOH/H_2O mixture (20 mL) and the solution was degassed with argon for 5 min, after which Et_3N (0.094 mL, 0.68 mmol) was added. The reaction mixture was refluxed under argon for 7 h in the dark, after which it was filtered hot over celite. The filtrate was evaporated under reduced pressure. Column chromatography purification was then performed over silica gel (eluent: 15:85 MeOH / DCM, Rf=0.4). The solvent was evaporated and the product was finally reprecipitated from ethanol and toluene to yield [**10**]Cl as a violet powder (95 mg, 32% yield). ^{1}H NMR (300 MHz, MeOD, 298 K, see Figure AIII.1 for proton notation) ^{1}H δ (ppm) 9.64 (d, *J* = 8.4 Hz, 1H, B8), 8.95 (dd, *J* = 20.5, 8.9 Hz, 2H, B3+B4), 8.66 (t, *m*, 3H, A3+T3'), 8.48 (d, *J* = 8.0 Hz, 2H, 3T), 8.25 (m, 3H, B5+A4+T4'), 8.00 – 7.75 (m, 7H, T4+B6+B7+A5+T6), 7.44 (t, *J* = 7.5 Hz, 1H, A6), 7.33 (m, 2H, T5), 7.20 (t, *J* = 8.0, 6.4 Hz, 1H, A7), 6.80 (d, *J* = 8.8 Hz, 1H, A8). ^{13}C NMR (75 MHz, $CDCl_3$) δ (ppm) 163.24+160.70+ 160.37+ 159.96 (T2+T2'+A2+B2), 153.87 (T6), 153.18+152.51 (A8a+B8b), 139.77(B4), 138.86 (T4), 137.74+136.84 (A4+B5), 132.05 (A7), 131.84+131.77 (6B+7B), 130.75+129.96 (A4a+B4a), 130.45+130.55 (A5+B8), 129.75 (T4'), 129.65 (A6), 128.37 (T5), 124.92 (T3), 124.86 (A8), 123.95 (T3'), 121.76+121.69 (A3+B3). *ES MS m/z (calc):* 626.0 (625.8 [M - Cl]$^+$). *UV-vis:* λ_{max} (ε in L·mol^{-1}·cm^{-1}) in MeOH: 571 nm (7400). Anal. Calcd for $C_{33}H_{23}Cl_2N_5Ru$: C, 59.91; H, 3.50; N, 10.59. Found: C, 60.15; H, 3.45; N, 10.54.

[Ru(terpy)(dmbpy)Cl]Cl ([12]Cl). [Ru(tpy)Cl_3] (500 mg, 1.13 mmol), dmbpy (209 mg, 1.13 mmol) and LiCl (50 mg, 1.2 mmol) were mixed in 3:1 EtOH/H_2O mixture (100 mL). The suspension was put under argon. Et_3N (0.25 mL, 1.8 mmol) was added and the reaction was refluxed for 20 hours. Then it was filtered hot over celite to remove insoluble byproducts. The filtrate was rotary evaporated, then purified over alumina in the dark (eluent: 1% MeOH / DCM). The product eluted from the column as the initial violet band (Rf=0.3). The solvent was evaporated and the solid was reprecipitated from 1% MeOH / DCM and Et_2O to yield [**12**]Cl as a dark violet powder (337 mg, 51 %). ^{1}H NMR (400 MHz, MeOD, 298 K, see Figure AIII.1 for proton assignment) δ (ppm) 8.58 (m, 3H, B5 + T3'), 8.50 (d, *J* = 8.1 Hz, 2H, T3), 8.29 (d, *J* = 8.1 Hz, 1H, A3), 8.20 (t, *J* = 7.9 Hz, 1H, B4), 8.11 – 8.02 (m, 3H, T6 + T4'), 7.97 (t, *J* = 7.4 Hz, 2H, T4), 7.81 (d, *J* = 7.8 Hz, 1H, T5), 7.58 (t, *J* = 7.9 Hz, 1H, A4), 7.48 – 7.40 (m, 2H, T5), 6.89 (d, *J* = 7.7 Hz, 1H, A5), 3.30 (s, 3H, B7), 1.52 (s, 3H, A7). ^{13}C NMR (300 MHz, MeOD, 298 K) δ (ppm) 168.91 (B6), 167.09 (A6), 161.57+161.54+161.40 (A2+T2+T2'), 159.36 (B2), 154.47 (T6), 138.72 (B4), 138.63 (T4), 137.66 (A4), 135.85 (T4'), 128.59 (B5), 128.53 (T5), 127.45 (A5), 124.83 (T3), 123.77 (T'3), 122.59 (C5), 122.33 (A3), 28.77 (B7), 23.74 (A7). *ES MS m/z (calc):* 553.81 (554.03 [M - Cl]$^+$), 259.33 (259.28 [M – 2 Cl]$^{2+}$). *UV-vis:* λ_{max} (ε in L·mol$^-$

^{1}.cm^{-1}) in MeOH: 504 nm (6400). Anal. Calcd for $C_{27}H_{23}Cl_2N_5Ru \cdot 2.5H_2O$: C, 51.11; H, 4.45; N, 11.04. Found: C, 51.98; H, 4.44; N, 11.05.

[Ru(terpy)(dcbpy)(Cl)]Cl ([11]Cl): See Chapter 2 and Appendix II.

AIII.2. ^{1}H NMR and proton attribution

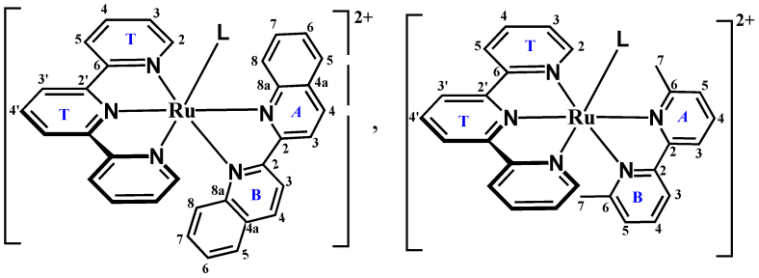

Figure AIII.1. Notations for the attribution of the ^{1}H and ^{13}C NMR spectra for compounds $[\mathbf{2}]^{2+}$, $[\mathbf{6}]^{2+}$, $[\mathbf{4}]^{2+}$, and $[\mathbf{8}]^{2+}$.

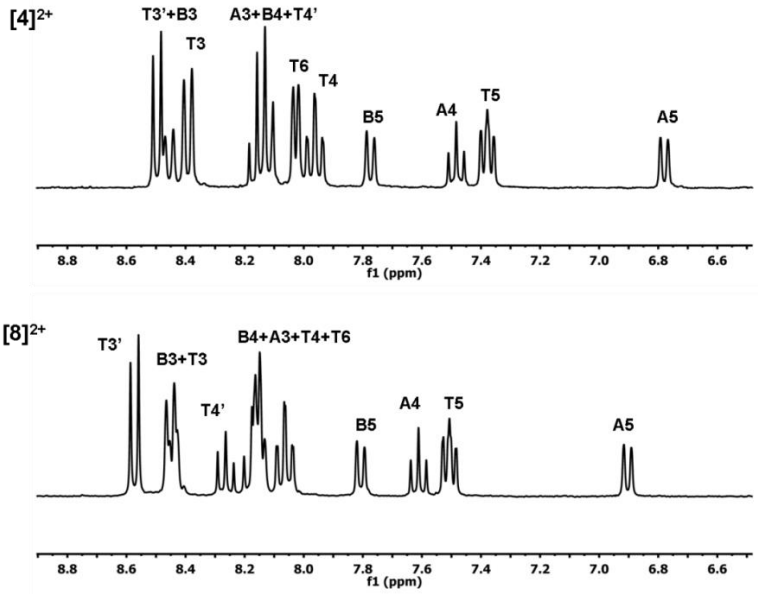

Figure AIII.2. ^{1}H NMR of $[\mathbf{4}]Cl_2$ (top) and $[\mathbf{8}]Cl_2$ (down) in pure D_2O (aromatic region, N-N=dmbpy). Conditions:$[Ru]_{tot}$=13.6 mM, *[Hmte]*=0 (top) or 0.53 M (bottom), pH ~ 7, 298 K.

AIII.3. X-ray crystallography for [5](PF$_6$)$_2$

All reflection intensities were measured at 110(2) K using a KM4/Xcalibur (detector: Sapphire3) with enhance graphite-monochromated Mo *K*α radiation (λ = 0.71073 Å) under the program CrysAlisPro (Version 1.171.34.36, Oxford Diffraction Ltd., 2010). The program CrysAlisPro (Version 1.171.34.36, Oxford Diffraction Ltd., 2010) was used to refine the cuvette dimensions. Data reduction was done using the program CrysAlisPro (Version 1.171.34.36, Oxford Diffraction Ltd., 2010). The structure was solved with the program SHELXS-97 (Sheldrick, 2008) and was refined on F^2 with SHELXL-97 (Sheldrick, 2008). Analytical numeric absorption corrections based on a multifaceted crystal model were applied using CrysAlisPro (Version 1.171.34.36, Oxford Diffraction Ltd., 2010). The temperature of the data collection was controlled using the system Cryojet (manufactured by Oxford Instruments). The H atoms were placed at calculated positions using the instructions AFIX 23, AFIX 43, AFIX 137 or AFIX 147 with isotropic displacement parameters having values 1.2 or 1.5 times *U*eq of the attached C or O atoms. The structure of [**5**](PF$_6$)$_2$ is mostly ordered. One of the two independent PF_6^- counter ions is found to be disordered over two orientations, and the occupancy factor of the major component refines to 0.906(4).

AIII.4. Aquation of hindered chlorido complexes in CD_3OD/D_2O mixtures

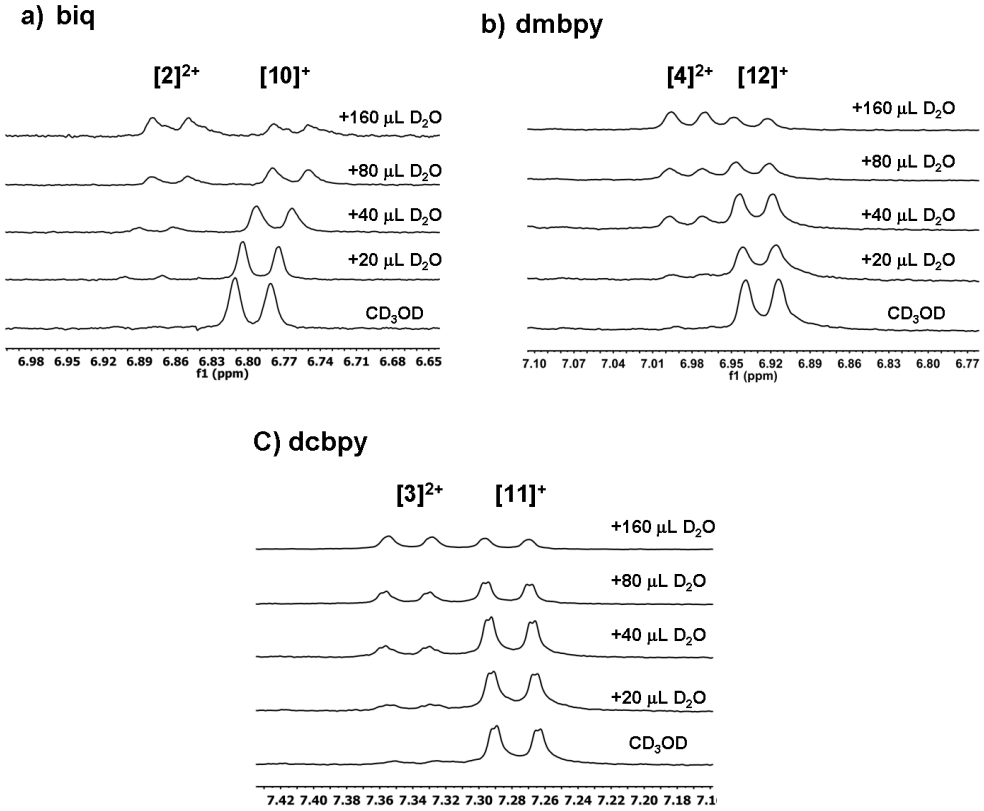

Figure AIII.3. ^{1}H NMR spectra showing the hydrolysis of [Ru(terpy)(N-N)(Cl)]Cl ([**10**]Cl, [**11**]Cl, and [**12**]Cl) upon addition of increasing amount of D_2O in MeOD. Conditions: a) initial $[Ru]_{tot}$=6.6×10^{-3} M, b) initial $[Ru]_{tot}$=9.2×10^{-3} M, and c) initial $[Ru]_{tot}$=9.6×10^{-3} M, T= 297K.

AIII.5. Determination of pKa of $[2]^{2+}$ and $[4]^{2+}$

pH titration: 3 mL of a 67 µM solution of [**10**]Cl or [**12**]Cl in perchloric acid (33 mM) was added to a UV-vis cell. A pH measurement electrode was added to the top and aliquots of aqueous NaOH (0.1 – 1 M) were added to give a range of pH values. After each addition of NaOH, the solution was stirred until a stable pH was observed, then a UV-vis spectrum was obtained. By deconvolution, the relative amounts of $[\mathbf{2}]^{2+}$ and $[\mathbf{4}]^{2+}$ were plotted *vs.* pH (Figure AIII.4). The data points were fitted to Equation AIII.1, which gave the pK_a of both

aqua complexes. The pK_a values were determined to be 9.5(1) and 10.5(1) for $[\mathbf{10}]^{2+}$ and $[\mathbf{12}]^{2+}$, respectively.

$$[RuOH_2]\% = \frac{a}{1 + 10^{-k(pH - pK_a)}} \quad \textbf{(Equation AIII.1)}$$

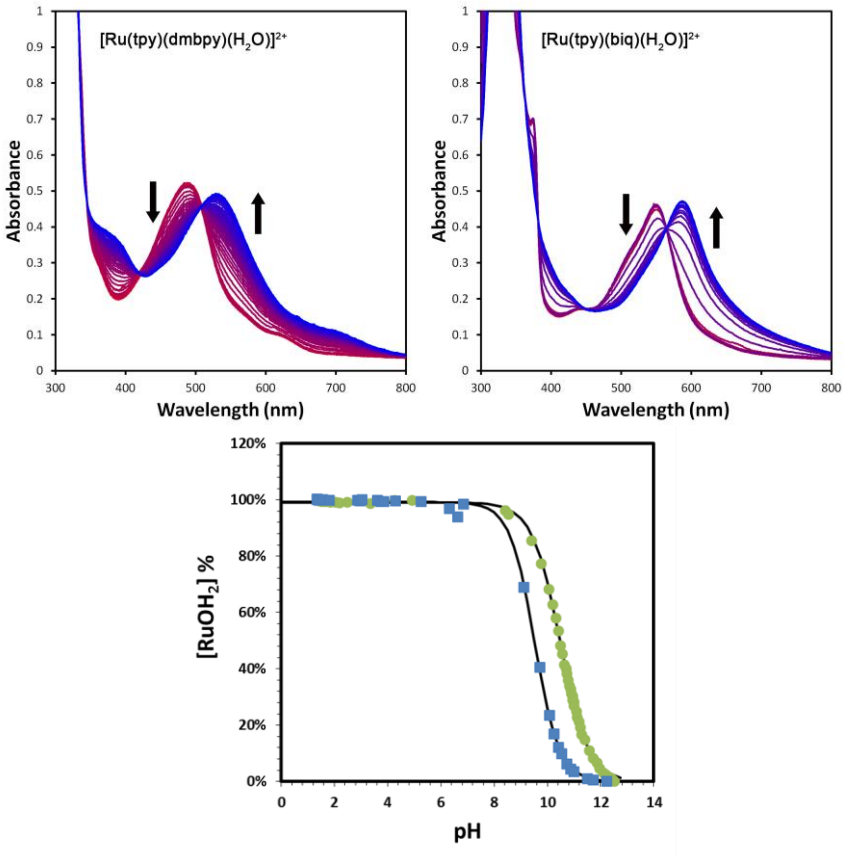

Figure AIII.4. tOP: Evolution of the UV-vis spectrum of $[\mathbf{2}]^{2+}$ and $[\mathbf{4}]^{2+}$ (67 µM) upon increasing pH using NaOH. Bottom: Composition (expressed in percent of the non-deprotonated species $RuOH_2$) during titration with NaOH. Squares: $[\mathbf{10}]^{2+}$, circles: $[\mathbf{12}]^{2+}$. Black lines: fit curves for the data points using Equation AIII.1.

AIII.6. Calculating the rate constants at different temperatures for the fast equilibrium between $[4]^{2+}$ and $[8]^{2+}$

If we consider the interconversion between $[\mathbf{4}]^{2+}$ and $[\mathbf{8}]^{2+}$ the rate law of this reaction can be expressed as Equation AIII.2.

$$\frac{d[RuHmte]}{dt} = k_4[RuOH_2] \cdot [Hmte] - k_{-4}[RuHmte] \quad \textbf{(Equation AIII.2)}$$

If pseudo first-order conditions are used (large excess of Hmte), since the concentration of Hmte is constant $k_4 \cdot [Hmte]$ can be replaced by the pseudo first-order rate constants k'_4 (see Equation 3.2 in the article).

Since k_{-4} is significant, $[RuOH_2]$ is substituted by $[Ru]_{tot} - [RuHmte]$ in Equation 3.2 (see Chapter 3), which simplified to Equation 3.3, where $k'_4 + k_{-4} = k_{obs}$ is usually called the "observed" rate constant (unit: s^{-1}).

Integration of this differential Equation 3.3 leads to Equation 3.4 (see Chapter 3), where c is a constant derived from integration.

Since there is no linear form of this formula, data had to be fitted with Equation AIII.3, using a non-linear least-squares minimization procedure as described by Lagarias *et al.*[2] (simplex search method). The program MATLAB was used for the optimization.

$$[RuHmte] = \frac{A}{B} - \frac{C}{B} \cdot e^{-B \cdot t} \quad \textbf{(Equation AIII.3)}$$

Figure AIII.5 shows a plot of the experimental data points, compared to the fitted model. The modeled curve closely matches the experimental data and thus $k'_4 = k_4 \cdot [Hmte]$ and k_{-4} could be calculated from the constants $A = k'_4 \cdot [Ru]_{tot}$ and $B = k_{obs} = k'_4 + k_{-4}$ determined numerically (see Table AIII.1).

Table AIII.1. The values of A, B, and C used as a model for Equation 3.4 and the kinetic data of the dmbpy system (equilibrium between $[\mathbf{4}]^{2+}$ and $[\mathbf{8}]^{2+}$) at different temperatures. Conditions: $[Ru]_{tot}$ = 1.5×10^{-4} M, *[Hmte]* = 3.2×10^{-2} M, MilliQ water, pH ~ 7.

T (K)	A	B	C	k_{-4} (s^{-1})	k_4 ($M^{-1} \cdot s^{-1}$)
283	7.6×10^{-8}	1.1×10^{-3}	2.7×10^{-8}	6.3×10^{-4}	1.6×10^{-2}
288	1.5×10^{-7}	2.3×10^{-3}	1.5×10^{-7}	1.4×10^{-3}	3.0×10^{-2}
293	2.7×10^{-7}	4.2×10^{-3}	2.6×10^{-7}	2.4×10^{-3}	5.4×10^{-2}
297	4.3×10^{-7}	6.9×10^{-3}	4.1×10^{-7}	4.1×10^{-3}	8.8×10^{-2}
301	7.4×10^{-7}	1.2×10^{-2}	6.5×10^{-7}	7.4×10^{-3}	1.5×10^{-2}

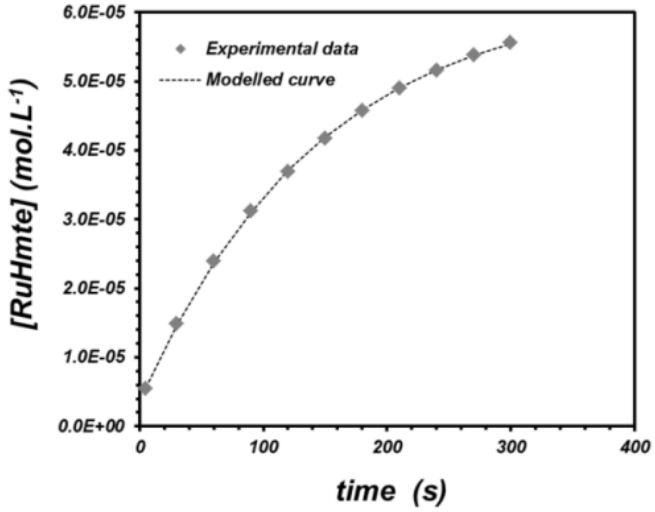

Figure AIII.5. Plot of *[RuHmte]* (concentration in $[\mathbf{8}]^{2+}$) *vs.* time during thermal substitution of H_2O by Hmte in complex $[Ru(terpy)(dmbpy)(H_2O)]^{2+}$ ($[\mathbf{4}]^{2+}$). Conditions: *[Hmte]* = 0.032 M, $[Ru]_{tot}$= 1.5×10^{-4} M, T = 297 K, in H_2O. Experimental data (diamonds) and calculated data (dashed curve).

Table AIII.2. Experimental pseudo first-order and second-order rate constants ($k'_i=k_i\cdot[Hmte]$ and k_i) at different temperatures for N-N=bpy, biq, and dcbpy. Condition: $[Ru]_{tot}=6.7\times10^{-5}$ M and $[Hmte]=6.7\times10^{-2}$ M for N-N=bpy and biq , $[Ru]_{tot}=1.4\times10^{-4}$ M and $[Hmte]=1.6\times10^{-1}$ M for N-N=dcbpy.

N-N	T (K)	k'_i (s^{-1})	k_i ($M^{-1}\cdot s^{-1}$)
bpy	323	5.4×10^{-5}	8.2×10^{-4}
	333	1.4×10^{-4}	2.1×10^{-3}
	343	3.7×10^{-4}	5.6×10^{-3}
	353	7.9×10^{-4}	1.2×10^{-2}
biq	297	4.3×10^{-4}	6.5×10^{-3}
	301	7.5×10^{-4}	1.1×10^{-2}
	308	1.7×10^{-3}	2.6×10^{-2}
	315	3.4×10^{-3}	5.2×10^{-2}
	323	6.2×10^{-3}	9.3×10^{-2}
	327	8.8×10^{-3}	1.3×10^{-1}
dcbpy	283	5.7×10^{-4}	3.6×10^{-3}
	288	1.1×10^{-3}	7.0×10^{-3}
	293	2.1×10^{-3}	1.3×10^{-2}
	297	3.6×10^{-3}	2.3×10^{-2}
	301	6.4×10^{-3}	4.0×10^{-2}

AIII.7. Order of Hmte and second-order rate constant determination at 297 K in the thermal coordination reaction for N-N=bpy, biq, and dmbpy

Stock solutions **θ** of complex [**1**]$(PF_6)_2$ (4.0 mg in 25 mL H_2O, 2.0×10^{-4} M), **ι** of [**10**]Cl (2.2 mg in 25 mL H_2O, 1.3×10^{-4} M), **κ** of [**12**]Cl (3.5 mg in 25 mL H_2O, 2.2×10^{-4} M), and **ξ** and **χ** of Hmte (600 mg in 25.0 mL H_2O, 2.60×10^{-1} M (**ξ**), and 1090 mg in 25.0 mL H_2O, 4.73×10^{-1} M (**χ**)) were prepared. 2.0 mL of **θ**, **ι,** or **κ** was added to a UV-vis cuvette, which was placed in the UV-vis spectrometer. The temperature was set at 50 °C for **θ**, and at 24°C for **ι,** or **κ**. After obtaining a constant temperature in each cuvette, to each solution was added x mL of H_2O, and 1-x mL of **ξ** or **χ**, where x is 0.2, 0.6, 0.8 or 1.0 mL of **ξ** to **θ**, and 0.2, 0.4, 0.8 or 1.0 mL of **χ** to **ι**, and 0.05, 0.10, 0.15 or 0.20 mL of **ξ** to **κ** . After addition of Hmte, a UV-vis spectrum was taken every 30 seconds. For each spectrum, the concentrations in *[RuHmte]* and $[RuOH_2]$ were determined by deconvolution of the UV-vis spectra knowing the extinction coefficients of both RuHmte and $RuOH_2$ species. For N-N=bpy and biq ($[\mathbf{1}]^{2+}$ and $[\mathbf{2}]^{2+}$) thermal back coordination (k_{-i}) is negligible and for each Hmte concentration the pseudo first order rate constants $k_{obs}=k_i\cdot[Hmte]$ were determined from the slope of the (linear) plot of $ln([RuOH_2]/[Ru]_{tot})$ *vs.* time (Figure AIII.6). For N-

N=dmbpy ([**4**]$^{2+}$), thermal back coordination is *not* negligible and as shown in Figure AIII.6c linear trend lines are not best fits for the data points. In such conditions k_{obs}= k_i·*[Hmte]*+k_{-i}, and a plot of *[RuHmte] vs.* time was obtained for each Hmte concentration. All the data were modeled to Equation AIII.3, and $A=k'_4\cdot[Ru]_{tot}$ and $B=k_{obs}=k'_4+k_{-4}$ were directly obtained from the model (see Equation 3.4). The plot of k_{obs} *vs. [Hmte]* was obtained for each N-N ligand (see Figure AIII.7). Finally, the second-order rate constant k_i were obtained from the slope of these plots for *i*=1 (bpy), 2 (biq), and 4 (dmbpy).

Half reaction times are calculated according to the Equation AIII.4.

$$t_{1/2(i)} = \frac{ln2}{k'_i} \quad \textbf{(Equation AIII.4)}$$

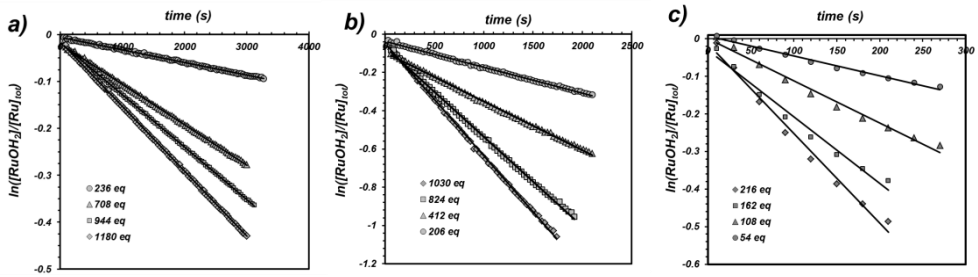

Figure AIII.6. Plot of *ln([RuOH$_2$]/[Ru]$_{tot}$) vs.* time for the coordination of Hmte to a) [**1**]$^{2+}$, b) [**2**]$^{2+}$, and c) [**4**]$^{2+}$ upon adding different equivalents of Hmte to the solution. Conditions: in water, pH~7, a) T=323 K, *[Ru]*$_{tot}$=1.3×10^{-4} M, b) T=297 K, *[Ru]*$_{tot}$=8.4×10^{-5} M , c) T=297 K, *[Ru]*$_{tot}$=1.5×10^{-4} M.

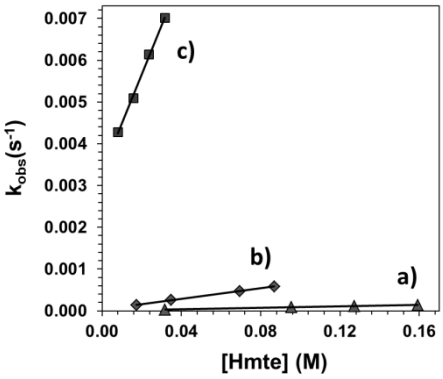

Figure AIII.7. Plot of *k'*$_i$ *vs. [Hmte]* in pseudo-first order conditions. a) N-N=bpy, slope= k_1=8.8×10^{-4} M^{-1}·s^{-1}, T=323 K, pH~7, *[Ru]*$_{tot}$=1.3×10^{-4} M, b) N-N=biq, slope=k_2=*6.4×10*$^{-3}$ M^{-1}·s^{-1}, *T*=297 K, *[Ru]*$_{tot}$=8.4×10^{-5} M , c) N-N=dmbpy, slope k_4=*0.12* M^{-1}·s^{-1}, T=297 K, *[Ru]*$_{tot}$=1.5×10^{-4} M.

AIII.8. Kinetics of the thermal hydrolysis of $[5]^{2+}$ (N-N=bpy) in MilliQ water at different temperatures

Table AIII.3. Experimental first-order rate constants (k_{-1}) at different temperatures for the thermal hydrolysis of $[\mathbf{5}]^{2+}$ in MilliQ water. Condition: $[Ru]_{tot}=2.5\times10^{-4}$ M.

T (K)	k_{-1} (s^{-1})
343	7.0×10^{-6}
348	1.2×10^{-5}
353	2.1×10^{-5}
358	4.3×10^{-5}
363	5.8×10^{-5}

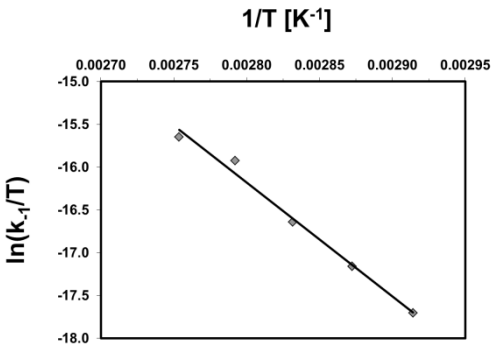

Figure AIII.8. Eyring plot for the thermal substitution of Hmte by an aqua ligand in $[\mathbf{5}]^{2+}$. The slope and y-intercept in the plot correspond to $-\Delta H^{\ddagger}_{-1}/R$, and $ln(k_b/h)+\Delta S^{\ddagger}_{-1}/R$, respectively. $\Delta H^{\ddagger}_{-1}$, $\Delta S^{\ddagger}_{-1}$, and $\Delta G^{\ddagger}_{-1}$ (at 297K) were found to be 110(6) kJ·mol^{-1}, –22(10) J·mol^{-1}·K^{-1}, and 117(10) kJ·mol^{-1}, respectively.

AIII.9. Quantum yield measurements for $[6](PF_6)_2$ and $[8](PF_6)_2$

Compound $[\mathbf{5}]^{2+}$ is kinetically stable and the photosubstitution quantum yield for this compound was calculated as explained in Appendix I, Section AI.3.1. (see Figure AIII.9).

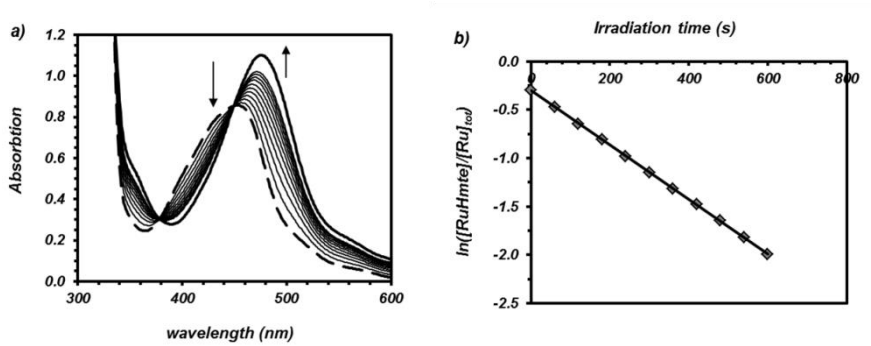

Figure AIII.9. a) Evolution of the UV-vis spectra of an aqueous solution of [**5**]$(PF_6)_2$ irradiated with blue light. Full conversion to [**1**]$(PF_6)_2$ is achieved within 30 minutes. Spectra were taken at 1, 2, 3, …, 10, and 30 minutes. b) Plot of $\ln([RuHmte]/[Ru]_{tot})$ *vs.* irradiation time. Condition: water, T=297 K, $[Ru]_{tot}$=1.0×10^{-4} M, λ_e=452 nm, photon flux Φ=6.4×10^{-9} Einstein·s^{-1}, slope $k_{\varphi i}$= 2.8×10^{-3} s^{-1}, ε_e=6000 L·mol^{-1}·cm^{-1}, A_e=0.88, and irradiation pathlength l'= 1 cm.

Compound [**6**]$^{2+}$ or [**8**]$^{2+}$ (RuHmte) are not kinetically stable and the equilibrium between RuHmte and $RuOH_2$ is fast, and the quantum yield cannot be measured for these compounds in a general way as reported in AI.3. In addition, isolation of [**6**]$(PF_6)_2$ or [**8**]$(PF_6)_2$ as pure solids was impossible. In order to perform quantum yield measurements a LED lamp was mounted on top of the UV-vis cuvette to irradiate the sample inside the UV-vis spectrometer. In such conditions, temperature stabilization issues during sample transfer are eliminated, and back-coordination of Hmte to $RuOH_2$ is minimized.

To measure φ_i, an aqueous solution of each complex [**10**]Cl or [**12**]Cl was prepared that contained a large excess of Hmte. After equilibration in the dark, the ratio $[RuHmte]/[RuOH_2]$ was measured by UV-vis spectroscopy; a value of 1.6 was found for the biq system and of 0.50 for the dmbpy system. The equilibrated samples were then subjected to visible light irradiation at room temperature at λ_e= 520 nm or λ_e=465 nm, respectively. In such conditions, three reactions take place simultaneously: 1) the photochemical cleavage of the Ru-S bond, 2) the thermal cleavage of the Ru-S bond, and 3) the thermal binding of Hmte back to the aqua complex (see Scheme 3.1). In such conditions, the variation of $[RuHmte]$ is given by Equation AIII.5, which can be rewritten for the thermal equilibrium in the dark (eq) into Equation 3.8a, and for the photochemical steady state (ss) into Equation 3.8b.

$$\frac{d[RuHmte]}{dt} = k_i[RuOH_2] \cdot [Hmte] - k_{-i}[RuHmte] - k_{\varphi i}[RuHmte] \quad \textbf{(Equation AIII.5)}$$

The plot of the ratio *[RuHmte]/[RuOH$_2$]* as a function of irradiation time was obtained by deconvolution of the UV-vis spectra using the extinction coefficients of RuHmte and RuOH$_2$. Since [**8**]$^{2+}$ (N-N=dmbpy) is involved in a very fast thermal equilibrium with [**4**]$^{2+}$, visible light irradiation did not change significantly the ratio *[RuHmte]/[RuOH$_2$]* during irradiation (see Figure AIII.10a), whereas for the biq system the thermal kinetics are lower and light irradiation leads to a photochemical steady state after about 1800 s irradiation. This steady state was characterized by a *[RuHmte]/[RuOH$_2$]* ratio of 0.10, which is very different from the ratio at the equilibrium in the dark (1.6, see Figure AIII.10b). Since k_i is known, k_{-i} could be calculated using Equation 3.8a. In a second stage, $k_{\varphi i}$ was obtained by using the values of k_i and k_{-i} in Equation 3.8b. The photochemical quantum yields were calculated using Equation 3.9, to give values of 0.12(5) and 0.30(6) for φ_2 and φ_4, respectively, at 297 K.

For comparison purposes φ_3 was also determined by the same method as for biq and dmbpy: an equilibrated solution of [**3**]$^{2+}$ and [**7**]$^{2+}$ was characterized by a *[RuHmte]/[RuOH$_2$]* ratio of 2.0, and in the steady state at λ_e= 465 nm a value of 0.13(5) was obtained for φ_3 (see Figure AIII.10c), which is consistent with the reported value in Chapter 2. All numerical parameters used to perform this calculation are indicated in Table AIII.4.

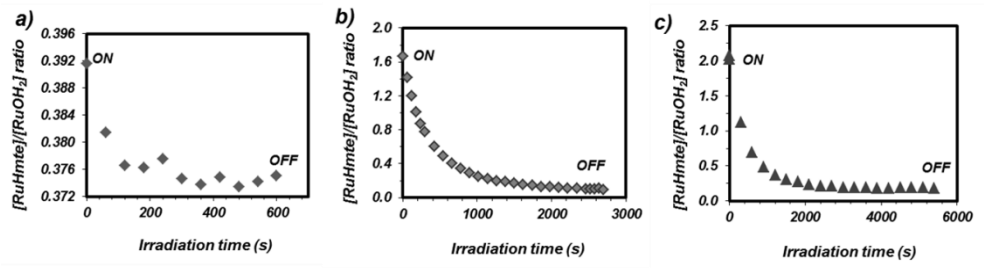

Figure AIII.10. Plots of the ratio *[RuHmte]/[RuOH$_2$] vs.* irradiation time for a) N-N=dmbpy ([**8**]$^{2+}$ ⇆ [**4**]$^{2+}$), Conditions: *T*= 297 K, blue light (λ_e=465 nm, photon flux Φ=4.0(4)×10^{-9} Einstein·s^{-1}), $[Ru]_{tot}$ = 1.9×10^{-4} M , *[Hmte]* = 0.20 M. b) N-N=biq ([**6**]$^{2+}$ ⇆ [**2**]$^{2+}$), Conditions: T= 297 K, green light (λ_e=520nm, photon flux Φ=9.8(5)×10^{-9} Einstein·s^{-1}), $[Ru]_{tot}$ = 8.6×10^{-5} M , *[Hmte]* = 0.011. c) N-N=dcbpy ([**7**]$^{2+}$ ⇆ [**3**]$^{2+}$), Conditions: *T*= 297 K, blue light (λ_e=465 nm, photon flux Φ=4.0(4)×10^{-9} Einstein·s^{-1}), $[Ru]_{tot}$ = 1.6×10^{-4} M, *[Hmte]* = 0.010 M. Spectra measured every 1 minute in all cases, pH~7.

Table AIII.4. Photochemical data for the calculation of the photosubstitution quantum yield for RuHmte complexes $[\mathbf{5}]^{2+}$, $[\mathbf{6}]^{2+}$and $[\mathbf{8}]^{2+}$. Conditions: T=297 K, MilliQ water, pH ~ 7.

	$[\mathbf{5}]^{2+}$	$[\mathbf{6}]^{2+}$	$[\mathbf{7}]^{2+}$	$[\mathbf{8}]^{2+}$
N-N	bpy	biq	dcbpy	dmbpy
$[RuHmte]/[RuOH_2]_{dark}$		1.6	2.0	0.392
$[RuHmte]/[RuOH_2]_{light}$		0.14	0.18	0.375
$[Hmte]$ (mol·L^{-1})		0.011	0.010	0.20
k'_i (s^{-1})		7.3×10^{-5}	2.2×10^{-4}	1.8×10^{-2}
k_{-i} (s^{-1})		4.4×10^{-5}	1.1×10^{-4}	4.5×10^{-2}
$k_{\varphi i}$ (s^{-1})	2.8×10^{-3}	4.2×10^{-4}	1.1×10^{-3}	2.0×10^{-3}
A_e	0.88	0.57	1.0	0.66
$[Ru]_{tot}$ (M)	1.5×10^{-4}	9.0×10^{-5}	1.5×10^{-4}	2.0×10^{-4}
λ_e (nm)	450	520	465	465
Photon flux Φ (Einstein·s^{-1})	6.4×10^{-8}	9.8×10^{-10}	3.9×10^{-9}	3.9×10^{-9}
φ_i	0.022	0.12	0.13	0.30

AIII.10. References

[1] C. A. Bessel, J. A. Margarucci, J. H. Acquaye, R. S. Rubino, J. Crandall, A. J. Jircitano, K. J. Takeuchi, *Inorg. Chem.* **1993**, *32*, 5779-5784.

[2] J. C. Lagarias, J. A. Reeds, M. H. Wright, P. E. Wright, **1998**, *9*, 112-147.

Appendix IV

Supporting Information of Chapter 4:

Binding of a ruthenium complex to a thioether ligand embedded in a negatively charged lipid bilayer:

a two-step mechanism

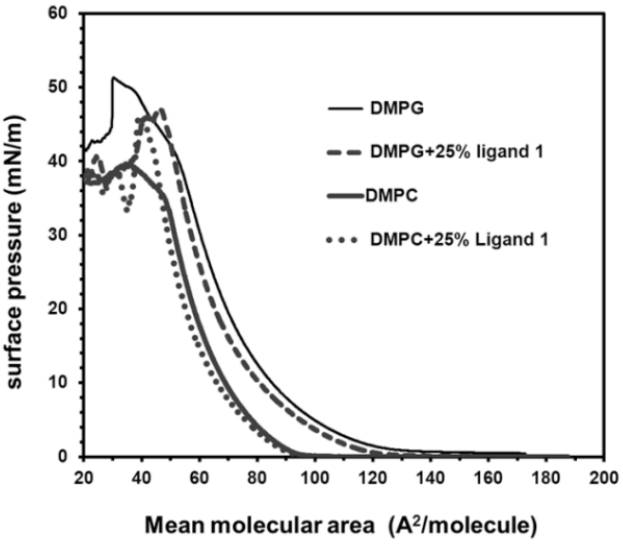

Figure AIV.1. Surface pressure *vs.* mean molecular area isotherms for the compression of lipid monolayers made of DMPG, DMPG with 25 mol% ligand **1**, DMPC, and DMPC containing 25 mol % ligand **1**, at the air/buffer interface. Compression rate: 2.4 mm/min, *T*=298 K, 10 mM phosphate buffer with *I*=50 mM, pH=7.0.

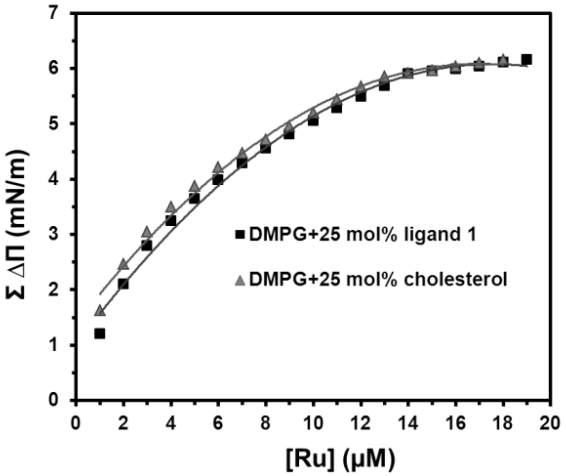

Figure AIV.2. Plot of surface pressure variation after each injection of $[\mathbf{2}]^{2+}$ *vs.* total concentration of $[\mathbf{2}]^{2+}$ in the trough upon titration of DMPG monolayers containing 25 mol% ligand **1**. Conditions: concentration of titrating $[\mathbf{2}](PF_6)_2$solution = 0.65 mM, *T*=298 K, lipid contents: 4.0 to 8.0 nmol.

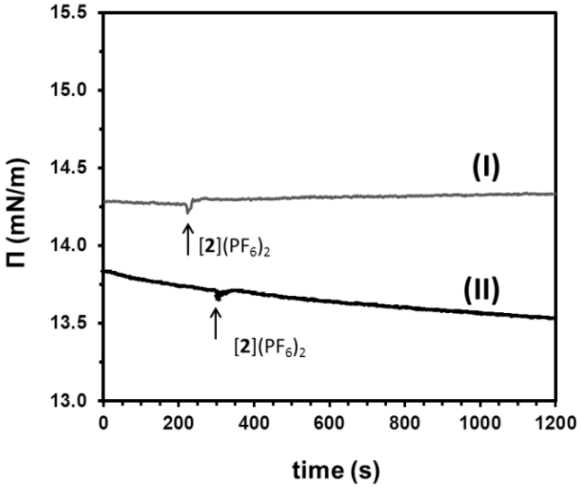

Figure AIV.3. Plots of surface pressure *vs.* time for zwitterionic monolayers after injection of $[\mathbf{2}]^{2+}$ (0.5 μM) into the buffer subphase: (I) DMPC and 25 mol % cholesterol, and (II) DOPC and 25 mol% ligand **1**. Each arrow represents the injection of 50 μL $[\mathbf{2}]^{2+}$. Conditions: concentration of titrating $[\mathbf{2}](PF_6)_2$ solution=0.65 mM, *T*=298 K, phosphate buffer: *I*=50 mM, pH=7.0, volume of the trough: 65 mL.

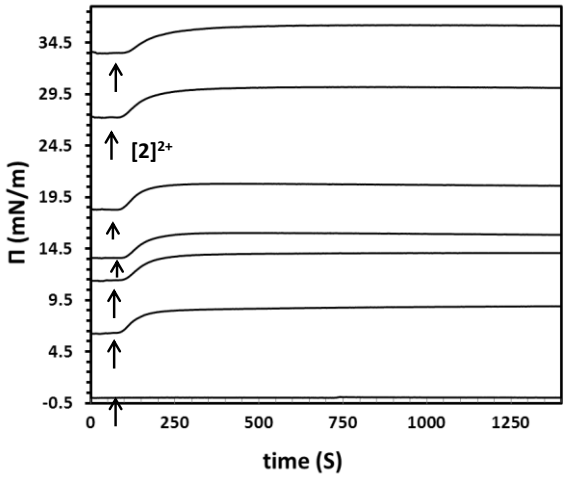

Figure AIV.4. Plots of surface pressure *vs.* time for DMPG monolayers containing 25 mol% of ligand 1 after injection of $[\mathbf{2}]^{2+}$ (3.5 μM) in a buffer subphase at different initial surface pressure Π_0. Condition: 10 mM phosphate buffer, total ionic strength=50 mM, concentration of $[\mathbf{2}]^{2+}$ in the stock solution=2.3 mM, *T*=298 K. At Π_0=0, there is no monolayer. Each arrow in the Figure shows an injection of 100 μL of $[\mathbf{2}]^{2+}$.

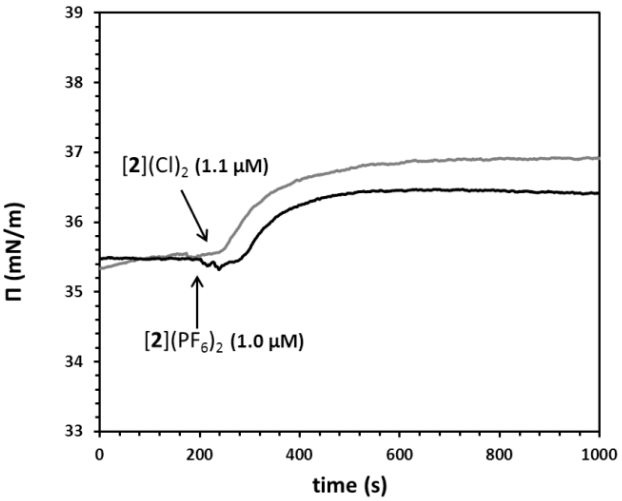

Figure AIV.5. Plots of surface pressure *vs.* time for a DMPG monolayer containing 25 mol% ligand 1 after injection of [**2**](PF$_6$)$_2$ (1.0 μM) or [**2**](Cl)$_2$ (1.1 μM) into a buffer subphase at an initial surface pressure Π_0~35.5 mN/m. Conditions: *I*=50 mM, concentrations of ruthenium stock solutions: 0.65 mM for [**2**](PF$_6$)$_2$, 3.5 mM for [**2**]Cl$_2$. T=298 K.

Table AIV.1. Thermodynamic data for the adsorption of [**2**](PF$_6$)$_2$ or [**2**]Cl$_2$ to DMPG liposomes functionalized with 25 mol% thioether-cholesterol ligand **1**. Conditions: ruthenium concentration = 0.62 mM, lipid concentration = 1.3 mM (as liposomes), phosphate buffer *I*=50 mM, pH=7.0, *T*=298 K.

Ruthenium complex	Apparent K_a (M^{-1})	$\Delta H°$ (kJ·mol^{-1})	$\Delta G°$ (kJ·mol^{-1})	$\Delta S°$ (kJ·mol^{-1}·K^{-1})	(Ru/lipid ratio) *n*
[**2**](PF$_6$)$_2$	1.5(7)×10^{+4}	58 ±9	−23	+275	0.18 ±0.01
[**2**]Cl$_2$	2.3(5)×10^{+4}	50±9	−25	+250	0.14 ±0.01

Appendix V

Supporting Information of Chapter 5:

Liposomes functionalized with ruthenium complexes: towards tumor-targeted light-controlled anticancer prodrugs

AV.1. Quantification of the quenching of NBD-PC fluorescence by ruthenium complex [1](PF$_6$)$_2$ supported on a liposome

In order to determine the amount of quenching of NBD-PC by the ruthenium complex [**1**](PF$_6$)$_2$ incorporated in PEGylated DOPC liposomes (DOPC:DSPE-PEG2K:NBD-PC (92:4:4) in PBS, the following procedure was performed. Liposomes that contained different amounts (0.5 to 5 mol%) of complex [**1**](PF$_6$)$_2$ were prepared as explained in section 5.5.3. A 24-well plate was prepared with liposome solutions in each well and the plate was read with a fluorescence spectrophotometer set at the excitation wavelength: 460 ± 5 nm and emission wavelength: 534 ± 5 nm. A plot of the fluorescent values *vs.* concentration of the ruthenium in each sample (mol%) was obtained (Figure AIV.1). The emission intensity of NBD-PC was found to be dependent on the amount of ruthenium present in the liposome membrane (expressed in mol% of the complex in the lipid formulation). The ruthenium concentration dependence was modeled as a second order polynomial (for ≤5 mol% Ru) as shown in Equation AV.1.

$$F = 0.038 \cdot [RuSRR']^2 - 0.36 \cdot [RuSRR'] + 1 \ (R^2 = 0.9968) \qquad \text{(Equation AV.1)}$$

In this equation, F is the fluorescence at $\lambda_{em.}$ = 534 nm ($F_{(0\ mol\%\ Ru)}$ = 100%) and *[RuSRR']* is the amount of [**1**](PF$_6$)$_2$ in mol% in the membrane.

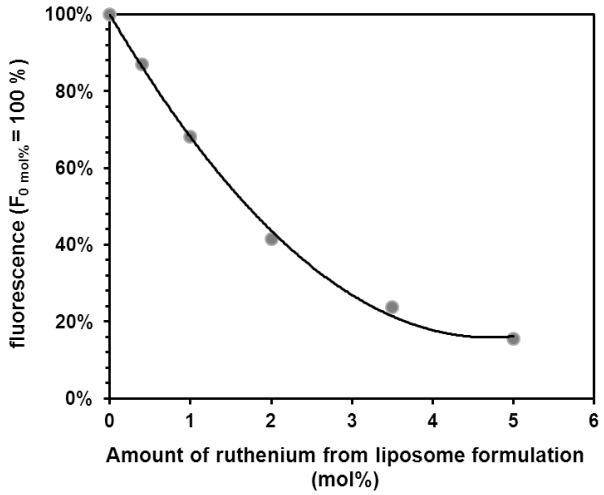

Figure AIV.1. Quenching of NBD-PC by different amounts of ruthenium complex [**1**](PF$_6$)$_2$ in mol% supported on DOPC:DSPE-PEG2K:NBD-PC(92:4:4) liposomes. Bulk total lipid concentration: = 2.5 mM (as liposomes), in PBS, *T* = 25 °C.

AV.2. Sample preparation protocol for ruthenium concentration measurement by ICP-OES

After cellular uptake of each liposome sample containing Ru, the cell lysis (in NaOH 0.2 M) was collected from each well and mixed together. 2.0 mL of the cell lysis was put in a glass reaction tube and 1000 µL of HNO_3 (65%) was added. The tube was closed by a glass marble. It was then put in an oven at 90 °C for 3 h, after which the digested sample was transferred to a volumetric flask and completed to 5.0 mL with Milli-Q. The clear solution was put in a corning tube and the ruthenium concentration was measured by ICP-OES. For all samples, the measured value for ruthenium concentration was lower than the sensitivity of the ICP-OES machine (*[Ru]*<20 ppb), while the concentration of the ruthenium in the liposome stock solution (before exposure to the cells) was measured to be about 3820(40) ppb in 5 mL digested solution (5 mol% Ru complex (*e.g.*, [**1**]$(PF_6)_2$) functionalized on liposomes, $[Ru]_{tot}$ = 0.075 mM, $[lipid]_{tot}$= 1.5 mM) . The expected concentration for 100% cellular uptake was 3870(40) ppb in 5 mL solution.

Table AV.1. Extinction coefficients of the ruthenium complexes at one wavelength. The values were used to calculate concentrations of *[RuSRR']* and $[RuOH_2]$ via deconvolution of UV-vis spectra.

Ru complex	[**1**]$^{2+}$		[**2**]$^{2+}$		[**3**]$^{2+}$		[**4**]$^{2+}$	
	RuSRR'	$RuOH_2$	RuSRR'	$RuOH_2$	RuSRR'	$RuOH_2$	RuSRR'	$RuOH_2$
ε ($L \cdot mol^{-1} \cdot cm^{-1}$)	4700	1000	4600	2400	5000	2100	5000	3100
λ (nm)	413		421		420		443	

Appendix VI

Supporting Information of Chapter 6:

Yellow-light sensitization of a ligand photosubstitution reaction in a ruthenium polypyridyl complex covalently bound to a rhodamine dye

AVI.1. ^{1}H NMR Spectra of the irradiated compounds

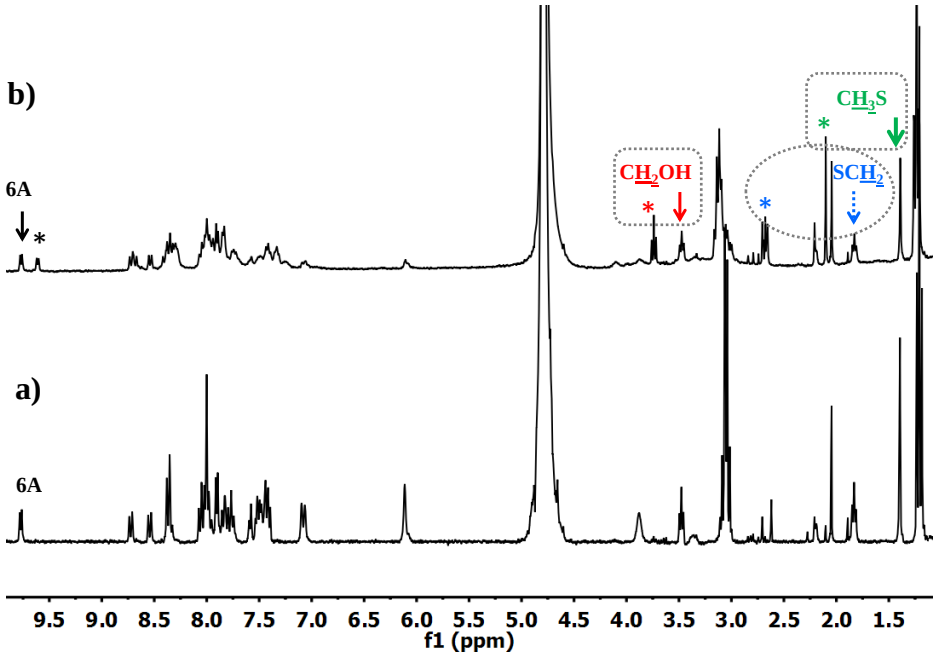

Figure AVI.1. ^{1}H NMR spectra of [**2**]Cl_3 (region 10–1.0 ppm) in D_2O before (a) and after (b) irradiation with yellow light for 530 min. The arrows show the peaks of coordinated Hmte and 6A in $[\mathbf{2}]^{3+}$, and the stars indicate free Hmte (aliphatic part) and 6A in $[Ru(\mathbf{4})(bpy)(D_2O)]^{3+}$ (aromatic part). Conditions: Yellow light irradiation (λ_e=570 nm, $\Delta\lambda_{1/2}$=8.9 nm, t=530 min, photon flux: 5.3×10^{-9} Einstein·s^{-1}), $[Ru]_{tot}=5.3\times10^{-3}$ M, T=298 K.

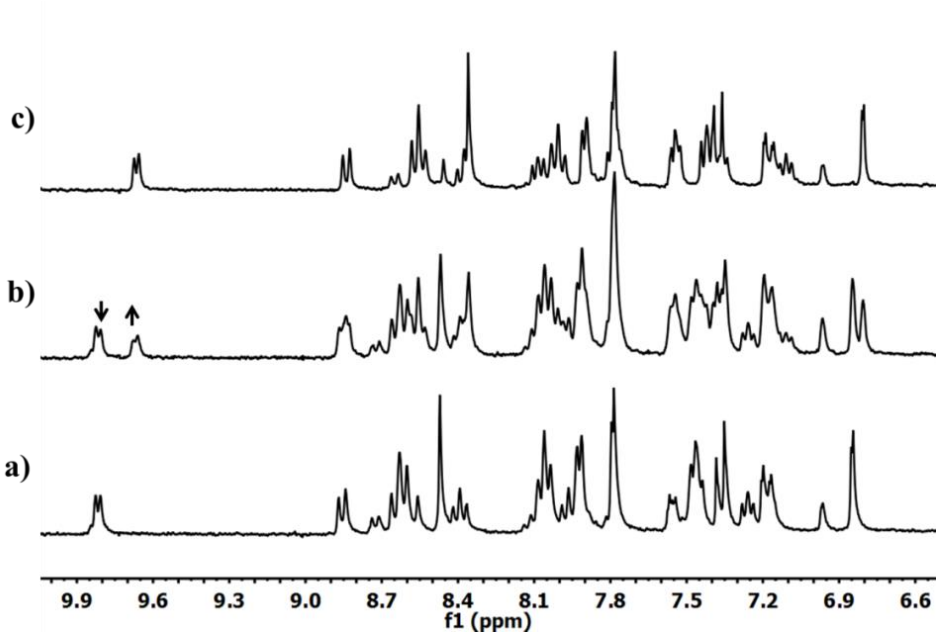

Figure AVI.2. ^{1}H NMR spectra of [**2**](PF$_6$)$_3$ (region 10–6.6 ppm) in acetone-d6/D$_2$O (90:10) (a) before irradiation and in the dark; (b) after 4 h irradiation with yellow light (λ_e=570 nm, $\Delta\lambda_{1/2}$=8.9 nm); the solution contains a mixture of [**2**]$^{3+}$ and [Ru(**4**)(bpy)(D$_2$O)]$^{3+}$; and (c) after leaving the sample under sun light for 2 days; full photoconversion to the aqua compound [**7**]$^{3+}$ was reached. Conditions: $[Ru]_{tot}$=2.0×10^{-3} M, T=298 K.

AVI.2. Photon flux determination

The photon flux for the irradiation setup at 452 nm was measured using the ferrioxalate actinometer.[1] However, the ferrioxalate actinometer is not suited for 570 nm photons, so that an indirect method was used. The light power (in mW·cm^{-2}) at 452 nm (I_{452}) and 570 nm (I_{570}) was measured using an OPHIR Nova power meter. Knowing the photon flux at 452 nm (Φ_{452}), the photon flux at 570 nm (Φ_{570}) was calculated using Equation AVI.1. In this equation E_λ is the photon energy at 452 nm (E_{452}=4.4×10^{-19} J) and at 570 nm (E_{570}=3.5×10^{-19} J). The photon flux at 570 nm was found to be 5.3×10^{-9} Einstein·s^{-1}.

$$\frac{I_{452}}{I_{572}} = \frac{\Phi_{452} \times E_{452}}{\Phi_{570} \times E_{570}} \qquad \textbf{(Equation AVI.1)}$$

AVI.3. References

[1] J. G. P. Calvert, J. N., *Chemical actinometer for the determination of ultraviolet light intensities. In Photochemistry*. Wiley and Sons, New York, **1967**, 780.